Electrochemical Resistive-Pulse Sensing of Extracellular Vesicles

Rui Jia,^{†,§} Susan A. Rotenberg,^{†,§} and Michael V. Mirkin^{†,#,*}

† Department of Chemistry and Biochemistry, Queens College-CUNY, Flushing, NY 11367, USA.

§ The Graduate Center of CUNY, New York, NY 10016.

Advanced Science Research Center at The Graduate Center, CUNY; New York, NY 10031.

*Corresponding Author

E-mail: <u>mmirkin@qc.cuny.edu</u>

FAX: 718-997-5531

Abstract

Extracellular vesicles (EVs) released from biological cells have attracted considerable interest due to their potential for cancer diagnostics and important role in cell signaling. Most previously reported studies have been concerned with the detection of EVs in biofluids and analysis of proteins and nucleic acids they contain. Electrochemical resistive-pulse (ERP) sensing enables direct detection of single EVs released from a specific cell and analysis of reactive oxygen and nitrogen species in such vesicles. Here we demonstrate the applicability of ERP sensing to distinguish between non-transformed and cancerous breast cell lines as well as between breast cancer cell lines with different metastatic potential. Another application of ERP sensing is in real-time monitoring of changes in a single cell induced by a chemical agent. This approach is potentially useful for evaluating the efficacy of therapeutic agents, including those that trigger breast cancer cell death by inducing intense oxidative stress.

A considerable research activity in the field of extracellular vesicles (EVs) is largely focused on their applications in diagnostics, ¹⁻⁵ and their roles in cell signaling ^{1,6} and cancer progression. ^{7,8} Most reported studies focused on EV detection in and separation from biofluids ⁹ and analysis of the proteins and nucleic acids they contain. ¹⁰⁻¹² Although useful and informative, these bulk measurements cannot trace an EV back to the cell from which it was released. Single-cell studies can provide real-time information about the dynamics of EV release, their functional heterogeneity, and enable characterization of the cellular redox status by analysis of vesicle contents. ^{13,14}

In this Article, electrochemical resistive-pulse (ERP) sensing¹⁵ was developed and applied to *in-situ* detect and analyze individual EVs released from a specific cell. ERP sensing is one of nanopipette-based electrochemical techniques developed for single-entity measurements. 16-19 It combines the advantages of conventional resistive-pulse sensing 20,21 and vesicle amperometry²²⁻²⁴ to detect single vesicles and analyze redox species contained inside them (see Experimental Section). In an ERP experiment (Figure 1a), an open carbon nanopipette (CNP) either unmodified (Figure S1b) or platinized (Figure S1c), serves as a working electrode. Only a small (µm-long) part of the CNP shaft adjacent to its orifice is filled with solution, and the measured signal is the faradaic current at the microscopic portion of the conductive film exposed to solution. A blockade of the diffusion current of redox species by a vesicle translocating through the CNP orifice results in a resistive pulse (green peak in the inset; Figure 1a). If a vesicle contains redox species (e.g., R in Figure 1a), the current upsurge caused by oxidation of R during its collision with the CNP inner wall (purple peak) follows the resistive pulse. CNPs have been used to measure reactive oxygen and nitrogen species (ROS/RNS)^{15,25} and catecholamine neurotransmitters²⁶ in single vesicles.

We recently reported electrochemical ROS/RNS sensing by inserting a nanoelectrode inside a living cell or positioning it near the cell surface. In this way, the ROS/RNS were measured in single vesicles inside murine macrophage cells.²⁷ As breast cancer progression is generally associated with high levels of ROS/RNS,²⁸ our previous nanoelectrochemical experiments revealed large amounts of ROS/RNS in metastatic breast cells in contrast to their low levels in non-transformed human breast cells.²⁹ Here we perform ERP sensing near the cell surface and demonstrate that ROS/RNS present in EVs can be used to distinguish non-transformed human breast cells from metastatic cells and differentiate between different breast cancer cell lines at the single cell level.

Previous nanoelectrochemical experiments performed inside an MCF-10A cell showed the increased production of ROS/RNS after the addition of DAG-lactone to the cell culture;²⁹ however, it was not clear whether the observed current spikes were produced by vesicle collisions with the electrode surface. Here we demonstrate that the produced ROS/RNS are stored in intracellular vesicles, and the resulting oxidative stress can be detected in real-time by ERP sensing of the released EVs. This approach is potentially useful for evaluating the efficiency of therapeutic agents.

EXPERIMENTAL

Chemicals and Materials. Phosphate buffered saline (PBS), potassium ferrocyanide (K₄[Fe(CN)]₆) and hexachloroplatinic acid (8 wt. %) were obtained from Sigma-Aldrich. Ferrocenemethanol (FcMeOH) and lead (II) acetate trihydrate (99.995%) were obtained from Alfa Aesar. All other chemicals were used as received. All aqueous solutions were prepared using deionized water from the Milli-Q Advantage A10 system (Millipore Corp.) equipped with

Q-Gard T2 Pak, a Quantum TEX cartridge and a VOC Pak with total organic carbon (TOC) ≤ 1 ppb. DAG-lactone (JH-131E-153) was a gift from Victor Marquez (NCI-Frederick).

Cell culture. MCF-10A cells were cultured in DMEM/F12 media (1:1) supplemented with 5% horse serum, 2% penicillin/streptomycin (PS), insulin (10 μg/ml), epidermal growth factor (20 ng/ml; Sigma-Aldrich), cholera toxin (100 ng/ml; Sigma-Aldrich), and hydrocortisone (0.025 μg/ml; Sigma-Aldrich), and fungizone (0.5 μg/ml). MDA-MB-231 cells (ATCC, Manassas, VA) were cultured in DMEM (ATCC) supplemented with 10% fetal bovine serum (FBS), 1% PS and fungizone (0.25 μg/mL). MDA-MB-468 cells were cultured in RPMI supplemented with 10% FBS, 1% PS and fungizone (0.25 μg/mL). The medium, serum and antibiotics were purchased from Invitrogen Life Technologies unless otherwise specified.

Cells were incubated at 37°C in a 5% CO₂ humidified atmosphere (D-6450 incubator, Heraeus) and passaged at a ratio of 1:5 to 1:8 every 2~3 days. Prior to electrochemical experiments, cells were plated at 5-10% confluence in a 60-mm tissue culture dish (Falcon) to obtain essentially isolated single cells. Prior to each experiment, adherent cells were rinsed and immersed in pH 7.4 PBS with/without redox mediators. For studies with DAG-lactone, PBS with redox mediators containing 10 μM DAG-lactone was used instead of culture medium.

Fabrication and characterization of quartz nanopipettes, CNPs and platinized CNPs. Nanopipettes with an orifice diameter from 150 nm to 800 nm were prepared by pulling quartz capillaries (1.0 mm o.d., 0.5/0.7 mm i.d.; Sutter Instrument Company) with a laser pipette puller (P-2000, Sutter Instruments). A thin layer of carbon was deposited on the inner wall of a nanopipette by chemical vapor deposition (Argon/Methane: 3/5) at 950°C for 20 min, as described previously. 15,30

Platinized CNPs were fabricated by electrodepositing Pt nanoparticles onto the inner carbon wall by 4-cycle potential sweep between 200 mV to -400 mV vs. Ag/AgCl with a 400 mV/s scan rate followed by the potential step to -80 mV. The constant voltage deposition was stopped when the current began to slowly grow and reached the 50-100 pA level. The platinizing solution was prepared by dissolving 1 mL of hexachloroplatinic acid (H₂PtCl₆, 8 wt. % in H₂O; Sigma-Aldrich) and 0.0016 g of lead(II) acetate trihydrate (Pb(OOCCH₃)₂•3H₂O, 99.995%; Alfa Aesar) in 6.4 mL of 10 mM PBS, and then diluting it with additional 44.8 mL of 10 mM PBS. The platinized CNPs were washed with distilled water.

After electrochemical resistive-pulse experiments, the size and geometry of a CNP were characterized by TEM (JEOL TEM-2100 Instrument) with an 80 kV voltage electron beam, as described previously. A quartz / carbon / platinized nanopipette was attached to the TEM grid (PELCO Hole Grids, copper) to make its tip visible in the grid center hole, and the rest of the pipette was cut off. A relatively low electron beam voltage of 80 kV was used to avoid damage to the pipettes. TEM images of representative quartz pipette, CNP, and platinized CNP are shown in Figure S1.

Positioning a nanopipette tip near the cell surface or inside the cell. A nanopipette was brought close to the cell membrane (or inserted into the cell cytoplasm) by using it as a scanning ion-conductance microscopy (SICM; in the case of a quartz pipette) or scanning electrochemical microscopy (SECM; in the case of a CNP) tip. The SICM/SECM experiments were carried out inside a Faraday cage using a previously described home-built instrument set on an optical table. A plastic 60-mm culture dish with adherent cells at low confluence was mounted on the horizontal stage of an Axiovert-S100 microscope (Zeiss) that was set on the same optical table. After placing a nanopipette above the cell using the inverted optical

microscope, the tip was moved vertically down to the cell surface (0.4 μ m/s approach velocity) by using a z-axis piezo actuator, and the approach curve (current vs. distance) was recorded.

With a quartz nanopipette used as an SICM tip, the measured ion current was inversely proportional to the resistance between the internal and external reference electrodes. When the nanopipette approached the cell surface, this resistance increased with decreasing separation distance between its orifice and the membrane. In the SICM current vs. distance curve (Figure S6), the ion current is essentially independent of the pipette tip position until the distance between the orifice and cell membrane (d) becomes comparable to the pipette radius. The separation distance between the pipette tip and the cell surface was evaluated from fitting the experimental approach curve to the theory. Unlike the intracellular measurements, the goal here was to avoid touching the cell membrane, and the approach in Figure S6 was stopped when the current decreased by <1%, corresponding to \sim 0.75 μ m distance. Consequently, the pipette was raised by 10 μ m.

With a CNP serving as an SECM tip, the solution contained $K_4[Fe(CN)_6]$ redox mediator. The base current was due to diffusion of $Fe(CN)_6^{4-}$ to the CNP orifice, which was blocked when the tip approached the cell membrane. The distance of the closest approach estimated from the fit of the experimental approach curve to the theory (Figure S7) was about 1 μ m, and the tip was raised by 10 μ m before making the resistive-pulse measurements of EVs.

ERP sensing inside a biological cell requires a hydrophobic redox species to partition into the cell cytoplasm from external solution and produce the base faradaic current. Thus, in intracellular ERP experiments, two redox mediators, i.e., relatively hydrophobic ferrocenemethanol and hydrophilic $K_4[Fe(CN)_6]$, were simultaneously present in solution, and the latter was used to facilitate the detection of cell penetration.²⁵

ERP and conventional resistive pulse sensing of vesicles. Resistive-pulse experiments were carried out with a patch clamp amplifier (Multiclamp 700B, Molecular Devices Corporation) in the voltage-clamp mode coupled with the home-built SECM instrument described above. A Digidata 1550A analog-to-digital converter (Molecular Devices) was used to digitize the signal at a sampling frequency of 100 kHz and a 2 kHz low pass filter frequency. The data was analyzed using pClamp 10 software (Molecular Devices).

In conventional resistive-pulse experiments, a quartz nanopipette was filled with solution from the back, an Ag/AgCl wire reference was inserted into the pipette, and voltage was applied between it and the external Ag/AgCl reference electrode (Figure S8a). 10 mM PBS solution (10 mM phosphate buffer, 2.7 mM KCl and 137 mM NaCl; pH 7.4) was used in resistive-pulse sensing of EVs.

In ERP experiments, a small amount of solution was drawn into the CNP through its tip by capillary forces, and its potential was controlled with respect to the Ag/AgCl external reference (Figure S8b). Solution contained 10 mM PBS (pH 7.4) and 10 mM K₄[Fe(CN)₆].

Fundamentals of conventional and electrochemical resistive-pulse experiments are outlined schematically in Figure S8 and Figure 1a. In a conventional resistive pulse experiment, the base ion current (i_0) through a quartz nanopipette is driven by voltage applied between two reference electrodes (Figure S8a), and vesicles are detected though ion current blockages caused by their translocations of nanopipette.^{20,31} Electrochemical resistive-pulse sensing of vesicles is shown schematically in Figure S8b. Unlike conventional resistive-pulse experiments, only a small (μ m-long) portion of the pipette shaft adjacent to its orifice is filled with solution, and no reference electrode is placed inside the CNP, which serves as a working electrode. The base current in this case is produced by diffusion of the redox species (e.g., ferrocyanide – a

hydrophobic ion present in the external solution that can neither partition inside the EVs nor enter the cell cytoplasm through the membrane) to the pipette orifice and their oxidation at the carbon surface. The blockage of this current during the vesicle translocation results in a resistive pulse (green peak in the inset; Figure S8b).

Platinized CNPs were used to combine ERP sensing with electroanalysis of reactive oxygen and nitrogen species (ROS/RNS) in a single vesicle (Figure 1a). Resistive-pulse recordings in this case are expected to include current blockages associated with vesicle translocations (green peak in Figure 1a) and current upsurges caused by oxidation of ROS/RNS during vesicle collisions with the CNP inner wall (purple peak). Because of the system geometry, all redox species released during the collision event are completely and rapidly oxidized (or reduced) at the platinized CNP surface. 32,33

Because the sources of the signal in ERP experiments (diffusion current of redox species to the CNP orifice) and conventional resistive-pulse sensing (ion current) are different, one can expect somewhat different EV frequencies to be measured for the same cell line with quartz and carbon pipettes. However, the experimentally measured differences turned out to be relatively small. For instance, the difference between the average EV frequencies measured for MCF-10A cells with quartz pipettes ($1.1 \pm 0.8 \text{ min}^{-1}$; 7 pipettes; 84 pulses; V = -400 mV) and CNPs ($1.9 \pm 0.5 \text{ min}^{-1}$; 8 platinized and 3 bare CNPs; 99 pulses; E = 850 mV vs. Ag/AgCl) is comparable to the experimental uncertainty margin. As discussed previously, 15 the voltage drop along the pipette axis inside its shaft is small because the conductive inner wall of a CNP is essentially equipotential, and the translocation of vesicles is driven by diffusion rather than electroosmosis or electrophoresis. Unlike conventional resistive-pulse experiments, in which the translocation of vesicles through the quartz pipette depends strongly on the applied voltage, ERP sensing is

essentially potential independent, which facilitates the comparison of current-time recordings obtained at different CNP potentials.

RESULTS AND DISCUSSION

ERP sensing of EVs released from single breast cells. Non-transformed human breast cells (MCF-10A; Figure 1b) and metastatic cancer cells (MDA-MB-231; Figure 1d) both release EVs, and the ERP frequency in the former case is only slightly lower (Table S1). The expulsion of EVs from MCF-10A cells was also confirmed by conventional resistive-pulse experiments (Figure S2). The blockage of the CNP orifice by a vesicle can also be visualized by TEM (Figure S3). The EV diameters measured using TEM (e.g., ~200 nm in Figure S3) are within the range of values determined for EVs released from MCF-10A and MDA-MB-231 cells by nanoparticle tracking analysis (50–400 nm).³⁴

Importantly, EVs released from MDA-MB-231 cells produce faradaic current spikes (Figures 1d and 1e), whereas there are few anodic spikes in the ERP recordings obtained with MCF-10A cells and their magnitude is relatively small (Figures 1b and 1c). Based on previous studies, 25,29 the faradaic current spikes can be attributed to oxidation of four primary ROS/RNS produced in breast cells, i.e., H_2O_2 , peroxynitrite (ONOO⁻), NO⁻, and nitrite ion (NO2⁻). The total charge per vesicle obtained by integrating the oxidation current under the faradaic current spikes recorded at the CNP potential, E = 850 mV vs. Ag/AgCl reference is 0.18 ± 0.04 pC (6 cells; 100 anodic current spikes) for MDA-MB-231 cells, and 0.018 ± 0.004 pC (5 cells; 38 current spikes) for MCF-10A cells. This 10-fold difference, reflecting the much larger amounts of ROS/RNS contained in EVs released from MDA-MB-231 cells, can be used to confidently differentiate between metastatic and non-transformed breast cells.

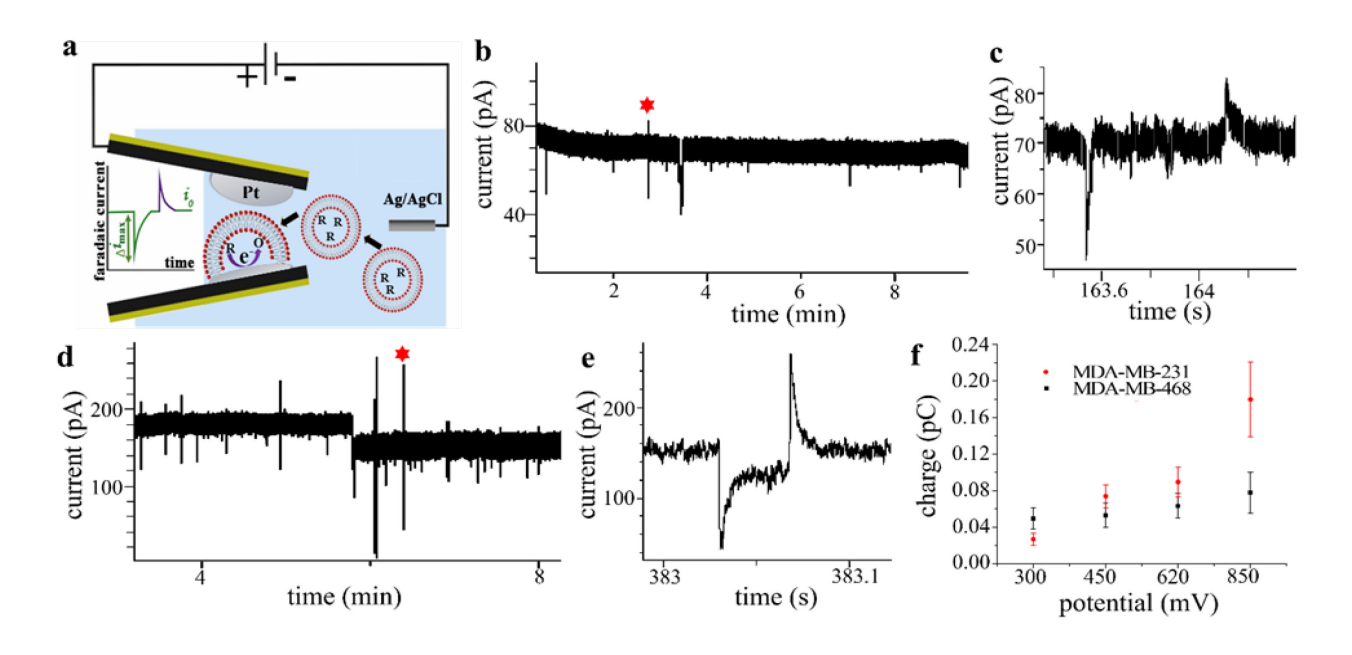


Figure 1. ERP sensing of EVs released from non-transformed and metastatic breast cells. (a) Schematic representation of an ERP experiment involving translocation of EVs through a platinized CNP. The inset shows faradaic current transient produced by the blockage of the CNP orifice (green peak) and oxidation of the redox species contained inside a vesicle (purple peak). (b,d) ERP current-time recordings obtained with a CNP positioned near MCF-10A (b) and MDA-MB-231 (d) cell surfaces. (c,e) Blowup of a representative current transient labeled by the red asterisk in (b) and (d), respectively. (f) Dependences of the mean ROS/RNS oxidation charge in a single EV on CNP potential for MDA-MB-231 (red) and MDA-MB-468 (black) cells. Error bars represent the 95% confidence intervals. (b-f) 10 mM PBS solution contained 10 mM K₄[Fe(CN)₆]. Platinized CNP diameter was 250 nm (b,c) and 414 nm (d,e).

To our knowledge, no measurement of ROS/RNS concentrations in EVs has been published to date. There is some indirect evidence that ROS may be present in cancer EVs that contain NADPH oxidase 2 (NOX2) complexes promoting ROS production.³⁵ Nitric oxide synthase (iNOS) detected in EVs³⁶ promotes RNS production. The total charge produced by ROS/RNS oxidation in single macrophage vesicles (phagolysosomes) was 0.23 pC.³⁷ This value is slightly higher than the 0.18 pC measured in EVs released from MDA-MB-231 cells.

Nanoelectrochemical measurements performed inside two different breast cancer cell lines (MDA-MB-231 and MDA-MB-468) with differing metastatic potential, ³⁸ showed strong correlation between intracellular ROS/RNS production and metastatic activity.²⁹ Using the approach developed by Amatore et al., 39 the contributions of individual ROS/RNS to the measured charge can be estimated from the current-time recordings obtained with platinized CNPs biased at different potentials roughly corresponding to the oxidation of H₂O₂ (300 mV vs. Ag/AgCl), H₂O₂ and ONOO (450 mV), H₂O₂, ONOO and NO (620 mV), and all four species (850 mV). For EVs released by MCF-10A cells, the faradaic current spikes at lower potentials are too small to measure. By contrast, for MDA-MB-231 cells (Figure S4) and MDA-MB-468 cells (Figure S5) the amounts of charge corresponding to individual ROS/RNS can be estimated from the ERP experiments carried out at different potentials. Figure 1f summarizing this data shows that only the average charge of H₂O₂ oxidation is slightly larger for EVs expelled from MDA-MB-468 cells, whereas the charges produced by oxidation of RNS (especially that of nitrite ion) are higher for EVs released by MDA-MB-231 cells. The total charge produced by oxidation of all ROS/RNS in a single EV at E = +0.85 V is 0.18 ± 0.04 pC for more aggressive MDA-MB-231 metastatic cells (100 EVs) and only 0.08 ± 0.02 pC for MDA-MB-468 cells (72 EVs). The t-test shows that this difference is statistically significant: the calculated t value (3.89) significantly exceeds the tabulated t either at the 95% (1.97) or the 99% (2.60) confidence level. This data also points to a strong correlation between the intracellular production rates and the amounts of ROS/RNS contained in EVs: intracellular voltammetry showed comparable levels of H₂O₂ in MDA-MB-468 and MDA-MB-231 cells, but much higher RNS levels in the latter (see Figure 5A in ref. 29). Our findings suggest that ERP sensing can be used to estimate the metastatic potential of breast cancer cells.

A much larger oxidation charge measured at 850 mV for EVs produced by MDA-MB-231 cells is in agreement with the finding of much higher RNS levels in MDA-MB-231 cells than in MDA-MB-468 cells reported in a previous study (ref. 29). Our data suggests that MDA-MB-231 EVs contain more nitrite ions than other ROS/RNS. Nitrite, which is oxidized at 850 mV, is a stable end product of NO metabolism, unlike the short-lived peroxynitrite species.

Establishing the one-to-one correspondence between a faradaic current spike and a resistive pulse is essential for identification and analysis of a specific vesicle. No such correlation was found in refs. 15 and 25, where the frequency of faradaic current spikes attributable to vesicle collisions was often larger than that of resistive pulses. This discrepancy was attributed to partial release of the vesicle contents during the collision event and/or undetected translocations of smaller vesicles that could produce immeasurably small current blockages. Figure 1d shows that one-to-one matching of a resistive pulse and a faradaic current spike produced by the same vesicle can be attained by careful deposition of the carbon film and Pt nanoparticles that have to cover the inner CNP wall all the way to its orifice (Figure S1c). Each recorded current transient comprises a resistive pulse caused by the vesicle translocation through the CNP orifice and immediately followed by the faradaic current spike due to ROS/RNS oxidation (Figure 1e). By analyzing an individual current transient, one can evaluate the size of a specific vesicle from the resistive pulse and determine its ROS/RNS contents from the faradaic current spike.

The delay between the resistive pulse and the corresponding faradaic spike represents the time between the vesicle's translocation through the orifice and its opening caused by a collision. Significant variations in the delay time can be expected because the trajectories of vesicles and their interactions with the platinized pipette wall are stochastic, and the time spent by a vesicle

inside the CNP may vary. The average EV translocation frequencies (Table S1) are \sim 1-2 min⁻¹, and a typical time gap between two vesicles is >10 s. Thus, with a typical delay between the resistive pulse and faradaic spike on the ms time scale (Fig. 1e) or even a few hundred ms delay (Fig. 1c), it is very likely that they are produced by the same vesicle. A much shorter delay (\sim 50 msec in Figure 1e vs. \sim 500 msec in Figure 1c) may be the reason why the current returned to the baseline value after the blockage in Figure 1c but remained lower than i_0 until the beginning of the faradaic spike in the Figure 1e. Apparently, in Figure 1e the delay time was too short for the vesicle to diffuse sufficiently far from the pipette orifice and stop blocking it. The current in Figure 1e eventually returned to the baseline value after the faradaic spike. It is also possible that some material transiently blocked the CNP orifice during the vesicle translocation in Figure 1e and then detached from the pipette wall and moved away from the aperture.

An important question is whether the differences in the charge measured for EVs released from different cell lines are due to different concentrations of ROS/RNS in those EVs or different vesicle sizes. For the same cell line, the increase in the average charge value with increasing potential (Figure 1f) is only due to the larger amounts of ROS/RNS molecules that get oxidized at more positive potentials since the average vesicle size is independent of the CNP bias. Conversely, the ROS/RNS oxidation charge measured for EVs released from the same cell using the same CNP biased at a constant potential tends to be higher for larger vesicles that produce higher ERP amplitude (Figure 2). Since the extent of the current blocking is a measure of the vesicle size, the correlation between the ERP pulse amplitude and faradaic charge and the ERP amplitude in Figure 2 suggests that the total amounts of ROS/RNS in EVs released from the same cell are largely determined by their size.

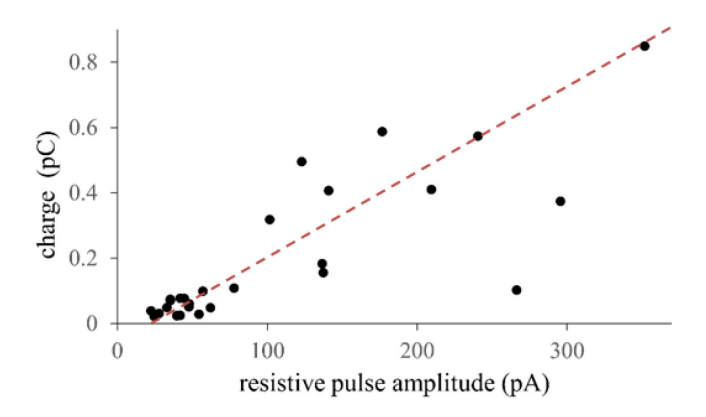


Figure 2. Relationship between the ROS/RNS oxidation charge measured during the collision of an EV with the CNP surface and the ERP amplitude produced by the same vesicle. EVs were released from an MDA-MB-231 cell and measured with a 414 nm-diameter platinized CNP at E = 850 mV vs. Ag/AgCl. The dashed line is drawn as a guide to the eye.

The comparison of average magnitudes of current blockages measured for different cell lines using similarly sized CNPs suggests that the differences in the average faradaic charge values are largely due to ROS/RNS concentrations rather than the vesicle size. In two sets of data shown in Table 1 the average values of the ERP amplitude measured for MCF-10A,

Table 1. Normalized resistive pulse amplitude and average oxidation charge per EV measured for different cell types

Cell type	Normalized ERP amplitude	Oxidation charge, pC	a, nm	No. of vesicles
MCF-10A	0.34 ± 0.18	0.006 ± 0.006	168	8
MDA-MB-468	0.29 ± 0.07	0.032 ± 0.010	220	11
MDA-MB-231	0.35 ± 0.11	0.130 ± 0.065	207	19
MCF-10A	0.17 ± 0.15	0.011 ± 0.002	385	8
MDA-MB-468	0.16 ± 0.05	0.066 ± 0.031	395	16
MDA-MB-231	0.14 ± 0.04	0.170 ± 0.076	342	17

10 mM PBS solution (pH 7.4) contained 10 mM $K_4[Fe(CN)_6]$. E = 850 mV vs. Ag/AgCl. Uncertainties are 95% confidence intervals.

MDA-MB-231, and MDA-MB-468 cells with comparable CNPs (pipette radius, $a \approx 200$ nm for the first three rows; and $a \approx 380$ nm for the last three rows) are very similar, but the corresponding oxidation charges are completely different. This data points to similar sizes of all types of EVs, but different total concentrations of ROS/RNS in them. The total concentration of ROS/RNS in EVs released from an MDA-MB-231 cell is higher than in those expelled from an MDA-MB-468 cell and much higher than in EVs produced by an MCF-10A cell.

Real-time monitoring of changes in the cell status induced by DAG-lactone. We employed ERP sensing of EVs for real-time monitoring of changes in the cell status induced by a chemical agent. The model process was the production of ROS/RNS in non-transformed MCF-10A cells induced by diacylglycerol-lactone (DAG-lactone) that can stimulate intracellular production of ROS/RNS presumably through activation of protein kinase C.⁴² Intense oxidative stress bursts were recorded previously with an intracellular nanoelectrode in ~25 min after treatment of MCF-10A cells with 10 μM DAG-lactone;²⁹ however, it was not clear whether the observed current spikes were produced by vesicle collisions with the electrode surface. ERP measurements inside a single MCF-10A cell performed under the same experimental conditions as in ref. 29 yielded a number of resistive pulses but no measurable anodic current spikes during the first 30 min after the addition of DAG-lactone to the bathing solution (Figure 3a). Later, the magnitude of the current blockages increased, and they became paired with anodic current spikes (Figures 3a,b), pointing to production of larger intracellular vesicles containing ROS/RNS.

ERP recordings obtained with a CNP positioned near an MCF-10A cell surface after adding DAG-lactone to the bathing solution contain a few resistive pulses and very small faradaic current spikes (Figure 3c). More frequent resistive pulses and much larger faradaic current spikes that appeared about 24 min after the addition of DAG-lactone are indicative of the

release of EVs loaded with ROS/RNS. The detection of these EVs is strongly correlated with the increased production of ROS/RNS in the cell. The capacity of ERP sensing to monitor chemical changes occurring in the cell in real time is potentially useful for evaluating the efficacy of therapeutic agents, including those aimed at inducing intense oxidative stress to trigger cell death. 43,44

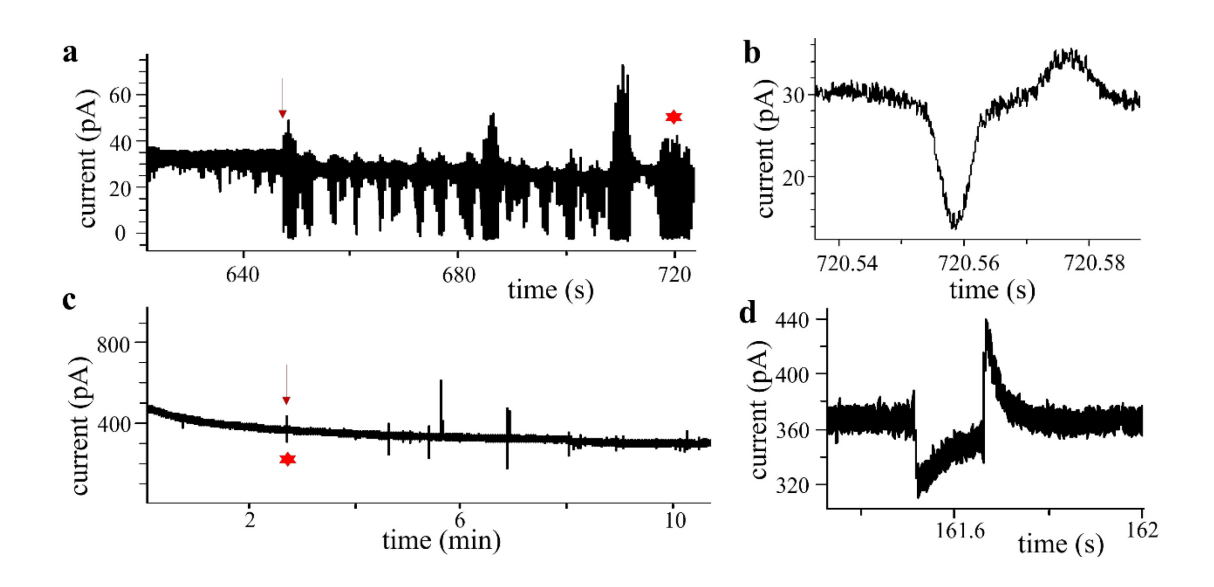


Figure 3. Monitoring ROS/RNS production in an MCF-10A human breast cell induced by addition of DAG-lactone via ERP sensing of intracellular (a) and extracellular (c) vesicles. E = +850 mV vs Ag/AgCl. (b,d) Blowup of a representative current transient labeled by the red asterisk in (a) and (c), respectively. Red arrow marks the first measurable faradaic current spike about 31 min (a) and 24 min (c) after adding DAG-lactone to the media. Platinized CNP diameter was 200 nm (a,b) and 600 nm (c,d). 10 mM PBS solution contained 1 mM FcMeOH, 10 mM K4[Fe(CN)₆], $10 \text{ }\mu$ M DAG-lactone and 0.1% v/v DMSO.

An important issue is the effect of the nanopipette size on the detection and analysis of EVs. It was shown previously that neither resistive pulses nor faradaic spikes can be measured if the radius of the pipette orifice (a) is smaller than that of the vesicle (a_v). Conversely, if $a \gg a_v$, the current blockage is weak, and the resistive pulses are obscured by the noise. Therefore, with a smaller nanopipette one records resistive pulses produced by smaller vesicles while not

detecting the larger ones; and a larger pipette can only detect larger vesicles. At the same time, the magnitude of a faradaic current spike is determined by the amount of electroactive species in the vesicle and should be essentially independent of the a_v/a ratio as long as the vesicle can translocate through the CNP orifice. Thus, we used CNPs with a larger than a_v of most vesicles in the population. Such large CNPs enabled the recording of faradaic current spikes produced by both larger and smaller EVs and the analysis of their contents. This strategy is not, however, suitable for intracellular ERP experiments because the insertion of a larger (e.g., a > 150 nm) pipette into a breast cell is likely to affect its viability. The high frequencies of both resistive pulses and faradaic spikes in Figure 3a suggest that many intracellular vesicles are sufficiently small to translocate through a 200-nm-diameter CNP.

Since EVs are released by immobilized cells, and their concentration in the bulk solution is negligibly low, there is a concentration gradient between the cell surface and the nanopipette that drives vesicle diffusion to the pipette orifice. Based on our system geometry, the collection efficiency (i.e., the ratio of the number of detected EVs to the number of EVs released from the cell) should be of the order of a few %, and its value should be comparable in different resistive-pulse experiments because of similar distances between the cell and the pipette, cell sizes, and pipette radii. A relatively low collection efficiency is not a big issue in this study because we aimed at sampling individual EVs rather than counting all EVs released from a cell.

The low collection efficiency contributed to a relatively low frequency of EV detection, which is orders of magnitude lower than the average detection frequency of intracellular vesicles (see Fig 3a and ref. 25). Although, the frequencies measured for a number of different cells are within 10-15% from each other (Table S1), suggesting reasonable accuracy and reproducibility of such measurements, the exact relationship between the numbers of detected EVs and those

released from a cell is not yet known, and the ERP frequency should not be used as a quantitative measure for comparing different cells.

CONCLUSIONS

ERP sensing is a new tool for probing the dynamics of EV release and studying EV chemistry and biology in vivo at the single-vesicle level. Using this technique, one can sample single EVs produced by a specific cell and analyse their contents. It allowed us to differentiate between non-transformed and cancer cells and between different lines of metastatic breast cells. Although intracellular amperometric experiments showed strong correlation between intracellular ROS/RNS production and metastatic activity, ²⁹ they are too hard and time consuming for cancer diagnostic. EVs released from different breast cell lines showed a similar trend, i.e., the larger total amount of ROS/RNS in vesicles corresponds to the higher metastatic potential of the cell. ERP detection and analysis of EVs are a suitable analytical platform for studying ROS/RNS-related carcinogenesis and are potentially useful for early diagnostics of aggressive triple-negative human breast cancers. EVs can also report on changes in the cell status induced by a chemical agent. Thus, we measured ROS/RNS in released EVs to monitor the oxidation stress in a single breast cell induced by adding DAG-lactone to the bathing solution. This approach is potentially useful for evaluating the efficacy of therapeutic agents.

Supporting Information

TEM images of CNEs, additional ERP recordings, SICM and SECM approach curves, and average frequencies of EV release, including Figures S1–S8 and Table S1 (PDF).

ACKNOWLEDGMENT

The support of this work by the National Science Foundation grant CHE-2102298 is gratefully acknowledged.

REFERENCES

- 1. Raposo, G.; Stahl, P. D. Extracellular Vesicles: A New Communication Paradigm? *Nat. Rev. Mol. Cell Biol.* **2019**, 20, 509-510.
- 2. Joyce, D. P.; Kerin, M. J.; Dwyer, R. M. Exosome-Encapsulated MicroRNAs as Circulating Biomarkers for Breast Cancer. *Int. J. Cancer* **2016**, 139, 1443-1448.
- 3. Xu, R.; Rai, A.; Chen, M.; Suwakulsiri, W.; Greening, D. W.; Simpson, R. J. Extracellular Vesicles in Cancer—Implications for Future Improvements in Cancer Care. *Nat. Rev. Clin. Oncol.* **2018**, 15, 617-638.
- 4. Théry, C. Diagnosis by Extracellular Vesicles. *Nature* **2015**, 523, 161-162.
- 5. Sheridan, C. Exosome Cancer Diagnostic Reaches Market. *Nat. Biotechnol.* **2016**, 34, 359-360.
- 6. Robbins, P. D.; Morelli, A. E. Regulation of Immune Responses by Extracellular Vesicles.

 Nat. Rev. Immunol. 2014, 14, 195-208.
- 7. Wortzel, I.; Dror, S.; Kenific, C. M.; Lyden, D. Exosome-Mediated Metastasis: Communication from a Distance. *Dev. Cell* **2019**, 49, 347-360.
- 8. Skog, J.; Würdinger, T.; Van Rijn, S.; Meijer, D. H.; Gainche, L.; Curry, W. T.; Carter, B. S.; Krichevsky, A. M.; Breakefield, X. O. Glioblastoma Microvesicles Transport RNA and Proteins that Promote Tumour Growth and Provide Diagnostic Biomarkers. *Nat. Cell Biol.* **2018**, 10, 1470-1476.
- Gardiner, C.; Vizio, D. D.; Sahoo, S.; Théry, C.; Witwer, K. W.; Wauben, M.; Hill, A. F.
 Techniques Used for the Isolation and Characterization of Extracellular Vesicles: Results of a
 Worldwide Survey. J. Extracell. Vesicles 2016, 5, 32945.

- 10. Shao, H.; Im, H.; Castro, C. M.; Breakefield, X.; Weissleder, R.; Lee, H. New Technologies for Analysis of Extracellular Vesicles. *Chem. Rev.* **2018**, 118, 1917-1950.
- 11. Yan, H.; Li, Y.; Cheng, S.; Zeng, Y. Advances in Analytical Technologies for Extracellular Vesicles. *Anal. Chem.* **2021**, 93, 4739-4774.
- 12. Zhu, Y.; Pick, H.; Gasilova, N.; Li, X.; Lin, T. E.; Laeubli, H. P.; Zippelius, A.; Ho, P. C.; Girault, H. H. MALDI Detection of Exosomes: A Potential Tool for Cancer Studies. *Chem* 2019, 5, 1318-1336.
- 13. Kalluri, R.; LeBleu, V. S. The Biology, Function, and Biomedical Applications of Exosomes. *Science* **2020**, 367, 6478.
- 14. Verweij, F. J.; Balaj, L.; Boulanger, C. M.; Carter, D. R. F.; Compeer, E. B.; D'angelo, G.; El Andaloussi, S.; Goetz, J. G.; Gross, J. C.; Hyenne, V.; Krämer-Albers, E. M.; Lai, C. P.; Loyer, X.; Marki, A.; Momma, S.; Nolte-'t Hoen, E. N. M.; Pegtel, D. M.; Peinado, H.; Raposo, G.; Rilla, K.; Tahara, H.; Théry, C; van Royen, M. E.; Vandenbroucke, R. E.; Wehman, A. M.; Witwer, K.; Wu, Z.; Wubbolts, R.; van Niel, G. The Power of Imaging to Understand Extracellular Vesicle Biology in Vivo. *Nat. Methods* **2021**, 18, 1013-1026.
- 15. Pan, R.; Hu, K.; Jiang, D.; Samuni, U.; Mirkin, M. V. Electrochemical Resistive-Pulse Sensing. J. Am. Chem. Soc. 2019, 141, 19555-19559.
- 16. Morris, C. A.; Friedman, A. K.; Baker, L. A. Applications of Nanopipettes in the Analytical Sciences. *Analyst* **2010**, *135*, 2190-2202.
- 17. Wang, Y.; Wang, D.; Mirkin, M. V. Resistive-Pulse and Rectification Sensing with Glass and Carbon Nanopipettes. *Proc. R. Soc. London Ser. A* **2017**, *473*, 20160931.
- 18. Zhang, S.; Li, M.; Su, B.; Shao, Y. Fabrication and Use of Nanopipettes in Chemical Analysis. *Annu. Rev. Anal. Chem.* **2018**, *11*, 265-286.

- Yu, R. J.; Ying, Y. L.; Gao, R.; Long, Y. T. Confined Nanopipette Sensing: From Single Molecules, Single Nanoparticles, to Single Cells. *Angew. Chem. Int. Ed.* 2019, *58*, 3706-3714.
- Bayley, H.; Martin, C. R. Resistive-Pulse Sensing from Microbes to Molecules. *Chem. Rev.* 2000, 100, 2575-2594.
- 21. Liu, Y.; Xu, C.; Chen, X.; Wang, J.; Yu, P.; Mao, L. Voltage-Driven Counting of Phospholipid Vesicles with Nanopipettes by Resistive-Pulse Principle. *Electrochem*. *Commun.* 2018, 89, 38-42.
- 22. Phan, N. T. N.; Li, X.; Ewing, A. G. Measuring Synaptic Vesicles Using Cellular Electrochemistry and Nanoscale Molecular Imaging. *Nat. Rev. Chem.* **2017**, 1, 1-18.
- 23. Li, Y. T.; Zhang, S. H.; Wang, L.; Xiao, R. R.; Liu, W.; Zhang, X. W.; Zhou, Z.; Amatore, C.; Huang, W. H. Nanoelectrode for Amperometric Monitoring of Individual Vesicular Exocytosis inside Single Synapses. *Angew. Chem. Int. Ed.* 2014, 53, 12456-12460.
- 24. Li, X.; Majdi, S.; Dunevall, J.; Fathali, H.; Ewing, A. G. Quantitative Measurement of Transmitters in Individual Vesicles in the Cytoplasm of Single Cells with Nanotip Electrodes. *Angew. Chem. Int. Ed.* 2015, 54, 11978-11982.
- 25. Pan, R.; Hu, K.; Jia, R.; Rotenberg, S. A.; Jiang, D.; Mirkin, M. V. Resistive-Pulse Sensing inside Single Living Cells. *J. Am. Chem. Soc.* **2020**, 142, 5778-5784.
- 26. Hu, K.; Jia, R.; Hatamie, A.; Le Vo, K. L.; Mirkin, M. V.; Ewing, A. G. Correlating Molecule Count and Release Kinetics with Vesicular Size Using Open Carbon Nanopipettes. *J. Am. Chem. Soc.* 2020, 142, 16910-16914.

- 27. Hu, K.; Li, Y.; Rotenberg, S. A.; Amatore, C.; Mirkin, M. V. Electrochemical Measurements of Reactive Oxygen and Nitrogen Species inside Single Phagolysosomes of Living Macrophages. *J. Am. Chem. Soc.* **2019**, 141, 4564-4568.
- 28. Heinecke, J. L.; Ridnour, L. A.; Cheng, R. Y. S.; Switzer, C. H.; Lizardo, M. M.; Khanna, C.; Glynn, S. A.; Hussain, S. P.; Young, H. A.; Ambs, S.; Wink, D. A. Tumor Microenvironment-Based Feed-Forward Regulation of NOS2 in Breast Cancer Progression. *Proc. Natl. Acad. Sci. U.S.A.* 2014, 111, 6323-6328.
- 29. Li, Y.; Hu, K.; Yu, Y.; Rotenberg, S. A.; Amatore, C.; Mirkin, M. V. Direct Electrochemical Measurements of Reactive Oxygen and Nitrogen Species in Nontransformed and Metastatic Human Breast Cells. *J. Am. Chem. Soc.* **2017**, 139, 13055-13062.
- 30. Hu, K.; Wang, Y.; Cai, H.; Mirkin, M. V.; Gao, Y.; Friedman, G.; Gogotsi, Y. Open Carbon Nanopipettes as Resistive-Pulse Sensors, Rectification Sensors and Electrochemical Nanoprobes. *Anal. Chem.* **2014**, 86, 8897-8901.
- 31. Luo, L.; German, S. R.; Lan, W. J.; Holden, D. A.; Mega, T. L.; White, H. S. Resistive-Pulse Analysis of Nanoparticles. *Annu. Rev. Anal. Chem.* **2014**, 7, 513-535.
- 32. Jia, R.; Mirkin, M. V. The Double Life of Conductive Nanopipette: A Nanopore and an Electrochemical Nanosensor. *Chem. Sci.* **2020**, 11, 9056-9066.
- 33. Lu, S.-M.; Peng, Y.-Y.; Ying, Y.-L.; Long, Y.-T. Electrochemical Sensing at a Confined Space. *Anal. Chem.* **2020**, 92, 5621-5644.
- 34. Yoshioka, Y.; Konishi, Y.; Kosaka, N.; Katsuda, T.; Kato, T.; Ochiya, T. Comparative Marker Analysis of Extracellular Vesicles in Different Human Cancer Types. *J. Extracell. Vesicles* 2013, 2, 20424.

- 35. Marar, C.; Starich, B.; Wirtz, D. Extracellular Vesicles in Immunomodulation and Tumor Progression. *Nat. Immunol.* **2021**, 22, 560–570.
- 36. Zhu, M.; Sun, X.; Qi, X.; Xia, L.; Wu, Y. Exosomes from High Glucose-treated Macrophages Activate Macrophages Andinduce Inflammatory Responses via NF-κB Signaling Pathway in Vitro and in Vivo. *Int. Immunopharmacol.* **2020**, 84, 106551.
- 37. Zhang, X. W.; Oleinick, A.; Jiang, H.; Liao, Q. L.; Qiu, Q. F.; Svir, I.; Liu, Y. L.; Amatore,
 C.; Huang, W. H. Electrochemical Monitoring of ROS/RNS Homeostasis within Individual
 Phagolysosomes inside Single Macrophages. *Angew. Chem. Int. Ed.* 2019, *58*, 7753-7756.
- 38. Cleris, L.; Daidone, M. G.; Fina, E.; Cappelletti, V. The Detection and Morphological Analysis of Circulating Tumor and Host Cells in Breast Cancer Xenograft Models. *Cells* **2019**, 8, 683-702.
- 39. Amatore, C.; Arbault, S.; Koh, A. C. W. Simultaneous Detection of Reactive Oxygen and Nitrogen Species Released by a Single Macrophage by Triple Potential-Step Chronoamperometry. *Anal. Chem.* **2010**, 82, 1411-1419.
- 40. Wang, Y.; Kececi, K.; Mirkin, M. V.; Mani, V.; Sardesai, N.; Rusling, J. F. Resistive-Pulse Measurements with Nanopipettes: Detection of Au Nanoparticles and Nanoparticle-Bound Anti-Peanut IgY. *Chem. Sci.* **2013**, 4, 655-663.
- 41. Terejánszky, P.; Makra, I.; Fürjes, P.; Gyurcsányi, R. E. Calibration-Less Sizing and Quantitation of Polymeric Nanoparticles and Viruses with Quartz Nanopipets. *Anal. Chem.* 2014, 86, 4688-4697.
- 42. Marquez, V. E.; Blumberg, P. M. Synthetic Diacylglycerols (DAG) and DAG-Lactones as Activators of Protein Kinase C (PK-C). *Acc. Chem. Res.* **2003**, 36, 434-443.

- 43. Trachootham, D.; Alexandre, J.; Huang, P. Targeting Cancer Cells by ROS-Mediated Mechanisms: A Radical Therapeutic Approach? *Nat. Rev. Drug Discov.* **2009**, 8, 579-591.
- 44. Kwon, S.; Ko, H.; You, D. G.; Kataoka, K.; Park, J. H. Nanomedicines for Reactive Oxygen Species Mediated Approach: An Emerging Paradigm for Cancer Treatment. *Acc. Chem. Res.* **2019**, 52, 1771-1782.

For TOC only

